JOURNAL - AUVSI SUAS 2016

Edhitha Unmanned Aerial Systems, M. S. Ramaiah Institute of Technology

Abstract

Edhitha has always been driven towards the goal of developing industry grade Unmanned Air Systems (UASs) suitable for a range of search and rescue, security, civilian and scientific research applications. *Team Edhitha* believes that autonomous UASs capable of image acquisition, data processing and communication, are a milestone in the field of artificially intelligent vehicles, and has therefore spent the past year pursuing full autonomy in all systems. For the SUAS 2016, the team has endeavoured to augment its UAS, already capable of autonomous flight, with complete automatic imagery and target detection capabilities. An emphasis was placed upon the development of a more robust data acquisition and processing system, and through a specially designed GUI, improve the monitoring of mission progress. *Team Edhitha* plans to attempt the Sense, Detect and Avoid task for the first time this year, and has spent a significant period of time to implement and optimize advanced path finding algorithms. Operator and system safety have been prioritized through the design process by minimizing points of failure and introducing redundancies to negate the effects of potential failures.

Contents

1.	**Description of Systems Engineering Approach**	
1.1	Mission Requirements Analysis	3
1.2	Design Rationale	
1.2.1	Airframe	3
1.3	Expected Task Performance	4
1.4	Programmatic Risks and Mitigation Methods	5
2.	**Description of UAS Design**	
2.1	Airframe	5
2.2	Power Systems	5
2.3	Flight Controller	6
2.4	Imagery System	6
2.5	Ground Control Station	6
2.5.1	Navigation Unit	6
2.5.2	Data Links	6
2.5.3	Communication and Data Processing Unit	8
2.6	Mission Planning	8
2.7	Data Processing	
2.7.1	Acquisition and Management of Images	9
2.7.2	Data Processing Algorithms and Target Types in ADLC	9
2.8	Interoperability	10
2.9	Sense, Detect, and Avoid (SDA)	10
2.10	Simulated Remote Information Center (SRIC)	11
3.	**Test Results And Performance At Mission Simulations**	
3.1	Navigation	11
3.2	Automatic Detection, Localization, and Classification (ADLC)	
3.2.1	Automatic Detection and Extraction of Targets	12
3.2.2	Colour Recognition	12
3.2.3	Shape Classification	12
3.2.4	Localization	12
3.2.5	QR Detection	12
3.3	Sense, Detect, and Avoid (SDA)	13
3.4	Simulated Remote Information Center	14
3.5	Interoperability	14
3.6	Performance of Airframe and Power Systems	15
3.7	Flight Controller	15
3.8	Data Transfer	15
3.9	Performance of Payload System	
3.9.1	On Board Computer	16
3.9.2	Imagery Performance	16
3.10	Summary of Test Results	17
4.	**Specific Safety Criteria for Systems and Operations**	
4.1	Safety Criteria for Systems	18
4.2	Safety Criteria for Operations	
4.2.1	Field Checklists	18
4.2.2	Navigation System Health Checks and Pre Arm Checks	18
4.2.3	Designated Tasks and Chain of Command	18
4.3	Safety Risks and Mitigation Methods	19
5.	**Conclusion**	19

1. Description Of Systems Engineering Approach

1.1 Mission Requirements Analysis

Edhitha's experience from previous editions of SUAS competition helped identify a set of objectives which, if achieved, would allow for the completion of most tasks. Through this approach, it was found that autonomous navigation, real-time image capture and processing, and a remotely controllable data exchange system gave the maximum possible flexibility in UAS performance. The rewards for the efforts and risks taken were considered, with the aforementioned capabilities having the highest reward for the least risk posed to the system. Autonomous navigation was the primary consideration, with all mission tasks based on the performance of the flight controller. In-flight re-tasking of the UAS was an additional feature that would allow for completion of the Emergent Target task and Sense, Detect, and Avoid. Remote image capture and wireless data transfer were next in our priority, for they allowed for the completion of maximum secondary tasks and expanded communication capabilities. System readiness for the above objectives, including an intelligent Ground Control Station (GCS) design, would ensure successful completion of the following tasks: Autonomous Navigation, Search Grid, Autonomous Detection, Localization, and Classification (ADLC), Actionable Intelligence, Emergent Target and Simulated Remote Information Center (SRIC). Based on the tasks planned, the requirements were analysed and the best fitting systems were chosen.

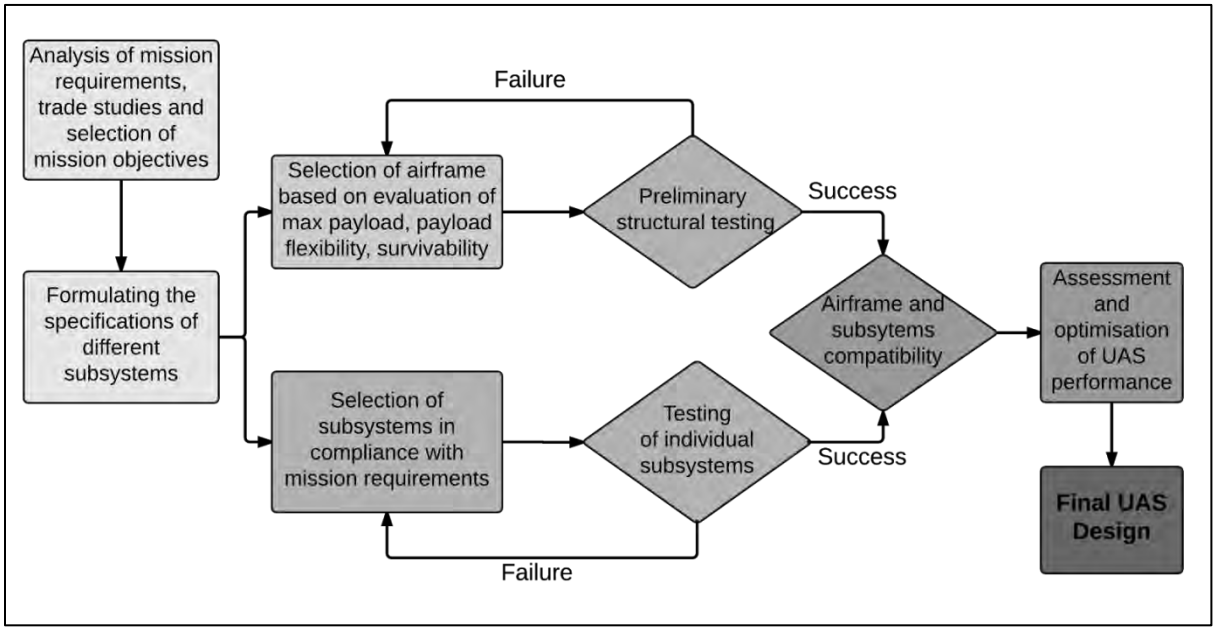

Fig. 1. Procedure for system design

1.2 Design Rationale

1.2.1 Airframe

The factors considered for airframe selection were airframe configuration, payload capacity, payload flexibility, survivability, and ease of transport. The configuration was a deciding factor, for it dictated the flight performance and also the ease of use of the airframe. Having used A-tailed and V-tailed airframes in the past, the team decided to use a conventional tailed airframe due to the comparable performance, but increased simplicity and minimized points of failure. Payload capacity and payload flexibility were primarily related to the size of the airframe. Payload flexibility was valued due to the use of a DSLR camera, which required a fuselage large enough to mount the camera without restricting access to other components on the UAS. Survivability was dictated by the material used.

Composite airframes had a low tolerance to crashes and hard landings, with foam airframes being more resilient and reparable. Ease of transport was determined by the dimensions of the disassembled UAS.
After an evaluation of airframes using the aforementioned factors, a conventional T-tail configuration airframe, propelled by twin electric motors was chosen. The fuselage offers sufficient accessibility to the camera and other systems, and allows for easy assembly and setup. The foam construction allows for quick repairs in the event of a crash, and has proven to sustain impacts that would cause complete structural failure in composite airframes. The low stall speed and glide characteristics favour endurance and suit the nature of the mission at the SUAS.

Table 1. Rationale behind system selection.

System	Options Considered	Product Chosen and Rationale
Electro Optical Imagery	**Nikon D3300** Point Grey Grasshopper Sony A6000 Sony RX100 Mk IV	**Nikon D3300** - High image resolution at 24.2 MP - High capacity battery - Compatibility with geotagger (**Solmeta Geotagger N3**) - Ease of integration with OBC
On Board Computer (OBC)	**Odroid C1** Odroid U3 PandaBoard Raspberry Pi B+	**Odroid C1** - 2 GHz 64 bit ARM v8 processor, with 2GB RAM with 4 USB 2.0 ports - Operates on Linux, compatible with available WiFi modules
Data Link	**Ubiquiti Bullet M5** **Ubiquiti Nanostation M5** Aerovironment DDL	**Ubiquiti Bullet M5** - Already in use and proven to work - Less expensive compared to the alternative - Couples with available **Ubiquiti Nanostation M5**
Flight Controller (FC)	**Pixhawk** APM 2.6 UAV Navigation Vector Cloud Cap Piccolo	**Pixhawk** - Open source nature allows for significant modifications - Extensive community support - Exceptional performance to cost ratio
Navigation GPS	**uBlox Neo 7M** uBlox LEA 6H	**uBlox Neo 7M** - Offers a refresh rate of 10Hz, much higher than the 5 Hz rate on alternative modules. - Cold start performance and positioning accuracy that are significantly better than the LEA 6H
SRIC Module	**Hardkernel WiFi Module** Ubiquiti Bullet M2	**Hardkernel WiFi Module** - Ease of integration with the OBC - Low physical footprint

1.3 Expected Task Performance

Component selection and UAS development were aimed at completion of all tasks with the exception of the off-axis and airdrop tasks, due to their low reward to risk ratio. Flight controller and payload operation were designed so as to achieve the objectives for all primary tasks. A larger focus was placed on major secondary tasks, those of ADLC, SRIC, Interoperability, and SDA. With the system having been designed for real-time image transfer and processing

capabilities, the UAS was expected to be able to meet the objective requirements for ADLC, Actionable Intelligence, and Emergent Target tasks. The interoperability setup was aimed at full server integration with all parameters to be delivered at required objective data rates. Integration of the object avoidance and path optimisation algorithm with the Flight Controller rendered the UAS capable of autonomous static obstacle avoidance. The SRIC payload and implementation were designed and expected to meet the autonomous SRIC task criteria.

1.4 Programmatic Risks and Mitigation Methods

A pseudo-quantitative risk analysis and characterisation has been performed, and the risk level has been determined by factoring in both the likelihood of a risk and its consequence, with the magnitude of the consequence being assigned a higher weightage. The assessment of risks has been followed by the development of comprehensive mitigation strategies.

Table 2. Risk Matrix: Programmatic risks and mitigation methods.

Risk	Likelihood	Impact	Mitigation Strategy
Loss of airframe	Low	High	Two backup airframes are kept ready at all times with one being flight ready.
Damage to airframe, and airframe components	Moderate	Low	Operational spares of all airframe components were acquired thus minimising development delay due to damage.
Complete loss of intellectual property	Low	High	All codes and designs were backed up regularly, and stored on a cloud storage server.
Sub System failure	Low	High	Backups were kept in multiples of two to account for any eventuality.

2. Description Of UAS Design

2.1 Airframe

The airframe has a 2.5 m wingspan with a conventional tail configuration. The airframe primarily consists of three separate wing sections, a detachable tail unit, fuselage, and three access panels. The mid wing section has been utilized to house the Flight Controller (FC) to enable ease of access and enhance modularity. The wing has been reinforced with carbon fibre spars to minimize flexure and to handle payloads beyond design limits. The added strength allows for high rates of roll and pitch without damage to the structure of the wing, thus allowing for evasive manoeuvres required to perform the Sense, Detect, and Avoid task.

2.2 Power Systems

The airframe is propelled by two brushless outrunner motors rated at 660W each. The motors are rated at a maximum current draw of 45 A each. The speed controllers used have been rated at 75A, operating at a factor of safety of 1.66 to handle unforeseen current spikes. The motors are rated for a thrust of 1.4 kg with a 10” X 6” propellor, thereby providing a total thrust of 2.8 kg with a twin motor configuration. The thrust to weight ratio for a fully loaded airframe is 0.45, which allows for steep climbs and manoeuvres.

Voltage regulators built into the speed controllers are used to provide primary power to the servos and auxiliary power to the flight controller. Each voltage regulator is rated at a constant 5 A current draw at voltages below 6 V. The voltage regulators operate at a factor of safety of 1.42, rendering them capable of handling the highest possible current draw of 3.5 A, a highly unlikely demand during normal operation. A 16000 mAh, 14.8 V Lithium Ion Polymer battery is used to power the propulsion and control systems. The battery is expected to allow for 35 minutes of flight in a full mission configuration, with room for 3 minutes of extra flight before a noticeable drop in supply

voltage. The OBC and data modem are powered by a 2200 mAh 11.1 V Lithium Polymer battery isolated from the main power line to compartmentalize potential power failures and isolate power line noise.

2.3 Flight Controller (FC)

The Pixhawk has been used as the Flight Controller (FC) due to its unparalleled processing power for the cost. The open source nature of the FC allows for constant community driven development. A state estimation algorithm has been used to augment the FC's performance. The use of the algorithm has shown improvements in attitude and altitude control during autonomous flight. Flight performance is monitored via a telemetry link which also allows for in-flight re-tasking. The controller is deemed capable of generating flight data at 10 Hz as required by the interoperability task. The FC uses a Proportional Integral Derivative (PID) controller to control the attitude of the UAS, and separate control loops to handle waypoint transition, altitude, and speed control. Additional control loops allow for fine tuning of flight performance to maximize navigational accuracy. The FC uses an externally mounted GPS module and compass for navigation for positioning and orientation with IMU data being used to determine the attitude. An Extended Kalman Filter (EKF) is used to determine sensor health and disregard erroneous sensor readings. The EKF also allows for sensor fusion to provide the FC with the most accurate data for navigation and control.

2.4 Imagery System

The imagery system consists of a DSLR camera controlled by an On Board Computer (OBC). The camera is triggered at specified intervals to obtain images with a suitable overlap, while minimizing redundant imaging. The images captured are transferred to the Ground Control Station (GCS) by the OBC through a datalink. Images are captured at a 12 MP resolution for faster data transfer and maximum reliability of the ADLC algorithm. The camera is interfaced with a geotagger to have the position, heading, and altitude of the UAS embedded into the captured images. The camera is capable of shooting at a rate of 1 frame per second, which allows for image capture with a 73% overlap at cruise speed to ensure no targets are lost. A 35 mm prime lens is used considering an altitude of 120 m to obtain imagery with minimum distortion and wide area coverage.

2.5 Ground Control Station (GCS)

The GCS has been divided into the navigation and data processing units. The navigation unit operates the 915 MHz telemetry link to communicate with the FC and relays telemetry data to the interoperability server. The data processing unit is linked to the datalink to control the OBC and acquire captured images. The targets identified are sent to the interoperability server via a local network.

2.5 Navigation Unit

The GCS communicates with the FC using Mission Planner, an open-source application for MAVlink based flight controllers. Mission Planner is interfaced with the interoperability server to post telemetry data. The GUI enables real time point-and-click waypoint editing, and simplifies the monitoring of critical flight characteristics. The navigation interface also allows for display of obstacles for the SDA task, and flight boundaries. The interface enables control loop tuning on the fly to modify flight characteristics. No fly zones are displayed with respect to the position of the UAS with rally points that the UAS will return to in the event of a geofence breach. The navigation interface also notifies the operator in the event of sensor data variance, as is shown in Fig. 3.

2.5.2 Data Links

2.4 GHz Link: The 2.4 GHz link provides remote control for manual flight, and is controlled by the safety pilot. A 2.4 GHz link is also used for the SRIC data connection.
915 MHz Link: The 915 MHz link is a telemetry link connected to the FC, and is controlled by the navigation GCS operator.
5.8 GHz Link: The Ubiquiti Nanostation M5, at the GCS, is paired with the Ubiquiti Bullet M5 on board the UAS to establish a 5.8 GHz data link with the UAS. The datalink enables remote control of the OBC to trigger and transfer images to the GCS during flight.

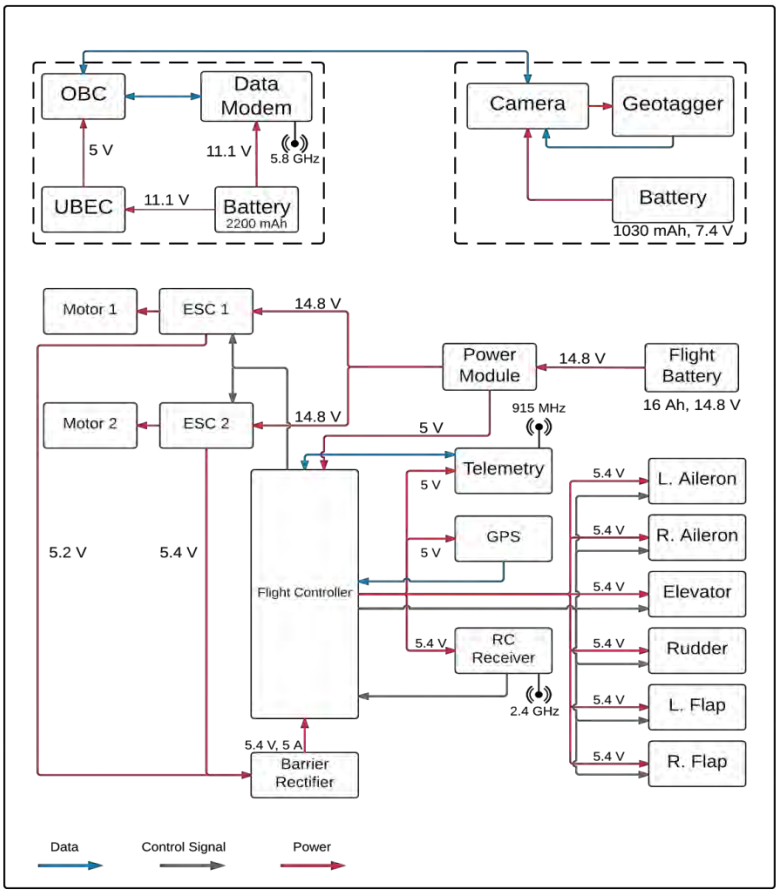

2.A.

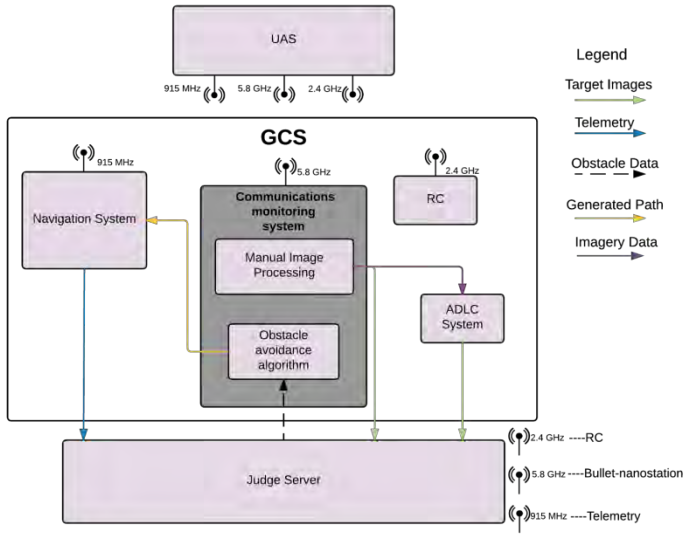

2.B.

Fig. 2.A. Block diagram representation of the UAS showing flow of power, data and control signals.
Fig. 2.B. Block diagram representation of the GCS showing flow of data.

2.5.3 Communications and Data Processing Unit

This unit interfaces with the On-Board Computer and enables image capture, data transfer, and processing of all collected data. Two systems handle all operations:

1. **Communications and Monitoring system (COM):** This system establishes a wireless link with the OBC via the 5.8 GHz communications link. The OBC which controls the camera transfers all imagery data to the GCS via the data link. The system enables a GCS operator to browse through images using a GUI, thus allowing manual target detection. The operator can also monitor the autonomous SRIC task wherein the OBC communicates with an external server.
2. **ADLC system:** The image processing algorithms are assigned a separate system that accepts incoming imagery data from the COM system and processes the images automatically. Detected targets and their characteristics are displayed on a GUI, and are sent to the interoperability server.

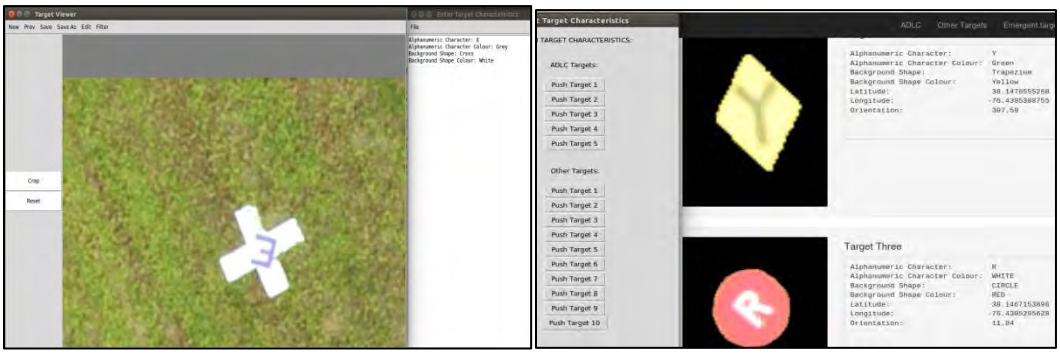

Fig. 3. (A, B) User Interface Units: A screenshot of the Manual Detection and Characterisation (Fig. 3.A.) and Automatic Detection, Classification, and Localisation (Fig. 4.B.) User Interfaces developed for SUAS 2016.

2.6 Mission Planning

Multiple search grids have been planned, each suited to wind conditions to minimize lateral drift. The altitude to be flown at has been set to 120 m, which allows the camera to cover a region of 88.071 m wide and 59.3 m tall in each frame. With the flight speed set to 16 m/s and the camera orientation, a 73% overlap will be seen at a capture rate of one frame per second. The overlap has been added to ensure no targets will be missed, and to increase the likelihood of a target being captured in more than a single image to allow for verification of target detection. A staggered search grid will be used to allow the UAS to execute banks at low angles, thereby reducing the potential for distortion in the captured images. A geofence will be set according to the data provided to ensure adherence to flight boundaries with rally points to which the UAS will return to in the event of geofence breach.

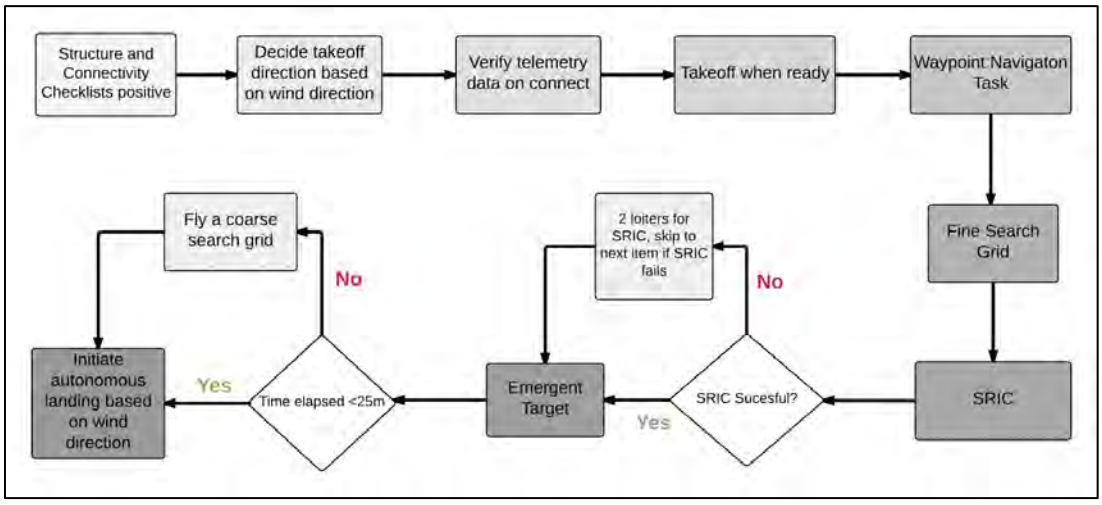

Fig.4. Mission Planning

2.7 Data Processing

2.7.1 Acquisition and Management of Images

The 5.8 GHz datalink allows GCS operators to remotely control the OBC, and through the OBC, extend control over the onboard camera. Linux kernel subsystems have been used to remotely trigger the camera, transfer a copy of the captured images from the OBC to GCS workstations, and to detect events in designated directories so that the images received can be processed asynchronously.

2.7.2 Data Processing Algorithms and Target Types in ADLC

Saliency Detection

The saliency detection algorithm detects regions of interest by comparing their contrast to surrounding areas. The first step in saliency detection is the conversion of the image to the lab colour space and the subtraction of the average pixel value (of the whole image) from each pixel of the converted image, thus producing a map of saliency. The image is then converted to a single channel image by taking the average of the three channel components. The resultant image represents a map of byte-sized pixel-salience values. The algorithm has been developed for images where the regions of interest are small in comparison to the background, and is therefore suited for mission requirements.

Selection of Potential Targets

The ADLC algorithm selects potential targets from all identified regions of interest based on a series of successive conditions or filters.

Area Filter

The *Area Filter* selects only those targets that satisfy a total pixel count within a range calculated using the target dimensions mentioned in the rules.

Colour Filter and Recognition

The *Colour Filter* selects targets based on the condition that any potential target would comprise of two dominant colours - the background colour, and the alphanumeric character colour. It also calculates the relative ratio of abundance between the two colours, and compares it to a range derived from the target data mentioned in the rules.
The *Colour Recognition* algorithm involves the processing of target images with the K-means clustering algorithm, followed by a conversion of the image to the HSV (Hue Saturation Variance) colour space to better classify different pixel values into different colour ranges.

Optical Character Recognition and Filter

The algorithm returns any identified character within the target dimensions (if any), with a confidence level. The threshold confidence level to establish a region of interest as a potential target has been empirically set to 85%.
The alphanumeric character is recognized using the Tesseract OCR engine, preferred over other OCR tools since it is independent of orientation, has an inbuilt confidence level, and a high quality of available documentation. The orientation of the character is then correlated with the original heading of the airframe (from image metadata) to derive the global orientation.

Shape Classification

The *Shape Classification* algorithm involves a reconstruction of the cropped target image using Probabilistic Hough Transforms and the subsequent classification of the reconstructed image. This classification has two stages. The first stage is an attempt to identify the shape depending on characteristic geometric parameters such as the number of vertices, the angles at the vertices, and the number of dominant sides. The second stage, called upon when the first stage fails, uses a template matching algorithm that returns the most probable shape out of the possible thirteen mentioned in the rules.

Localization

Using the local image coordinates of each detected target from image metadata, the distances in meters and orientations in degrees are obtained and passed to GeographicLib, a set of C++ classes to perform geodesic calculations conforming to the WGS84 standard, which yields output latitude, longitude, and altitude values.

Fail-safe

The fail-safe exists in case an image containing a potential target does not pass through the filters successfully. The images that are received at the GCS from the on-board camera are displayed on a UI, and are manually scrutinized for potential targets.

QR Code

The QR code is considered as a special case target. The *Area Filter* is modified to suit the specifications mentioned in the rules, and the colour filter is tuned to detect objects that are composed of only black and white blocks (squares). Once the QR target is obtained, the image is enhanced and passed to a code that uses an open source QR decoder.

Fig. 5. (A, B) Selection of potential targets: An example of the output result (**Fig. 5.B**) after the original image (**Fig. 5.A**, here, shown as a cropped version of the original image to highlight target) is passed through Saliency Detection and the aforementioned Filters.

2.8. Interoperability

Python scripts for the interoperability task perform login, download of server time, retrieval of obstacle data, and posting of UAS telemetry data using GET and POST requests. Telemetry upload, retrieval are performed parallely at an average rate of 10 Hz. The obstacle data is routed to the SDA algorithm to recalculate flight paths for obstacle avoidance, while the telemetry data, obtained from Mission Planner is pushed to the interoperability server. The errors returned by the server are displayed at the GCS, along with a constant stream of server timestamps.

2.9 Sense, Detect, and Avoid (SDA)

The path finding algorithm for the SDA task uses an iterative approach to generate multiple paths, and subsequently chooses the optimum path between two waypoints. The algorithm effectively simulates the behaviour of a flock of birds by having a population of candidate solutions move through the search-space while actively avoiding any obstacle in its path. In every iteration, the movement of an individual candidate is influenced by its own local position and the best known position found by other candidates. These best known positions are sampled at equal intervals to derive new waypoints that are communicated to the FC as a modified flight plan. The algorithm is modelled as an optimisation problem of minimising the distance to the destination. According to mission requirements, the admittance of obstacles was modified to allow for rerouting without requiring a deviation of more than 50 feet from the original path.

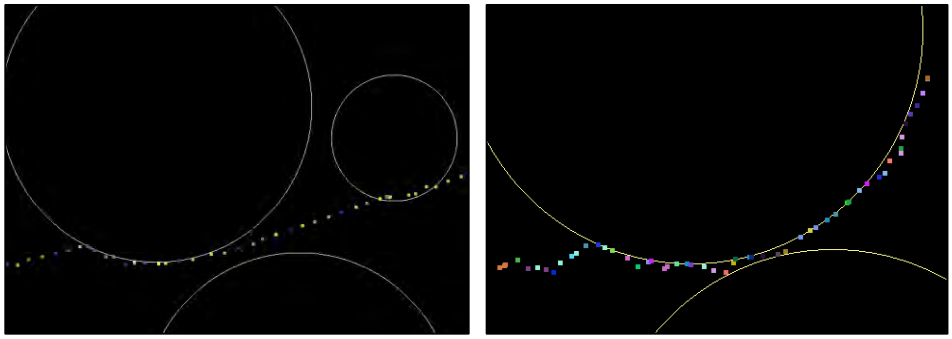

Fig. 6. (A, B) OpenGL simulation showing the implementation and optimisation of the path finding algorithm. **Fig. 6.A** [*left*] shows the initial algorithm failing in the scenario of multiple obstacles lying close to each other. Upon further calibration of certain parameters, the algorithm proves successful in plotting paths even through narrow gaps (**Fig. 6.B** [*right*]).

2.10 SRIC

The SRIC WiFi Module is connected to the OBC. The OBC automatically connects to the SRIC server via the WiFi module. The OBC then runs file transfer scripts via SFTP to upload and download files.

3. Test Results And Performance At Mission Simulations

3.1 Navigation

Initial tests showed acceptable path tracking with subpar waypoint capture. This was attributed to a poorly calibrated airspeed sensor leading to poor speed control. After calibration, target speeds were held within 2 m/s of the desired speed. Waypoint capture and transition were improved significantly after the calibration. Flight performance was tested with tuning gains obtained by manual and automatic methods with the automatic method providing a better result. The *L1* control loop and the *Total Energy Control System (TECS)* were tuned to optimize waypoint transitions and altitude control. The result of tuning was an airframe capable of capturing waypoints with an accuracy of 5 m within an altitude of 4 m. Maximum crosstrack error was lower than 10 m, well below the maximum value specified in the rules.

Autonomous landing was tested with a focus on altitude control. The TECS algorithm was used to achieve a perfect glide slope with accuracy in landing at a desired point. Ideal sink rates were computed and experimentally verified. Autonomous takeoffs were successful, with the UAS gaining the requisite altitude over a short distance, a capability afforded by the 0.45 thrust to weight ratio.

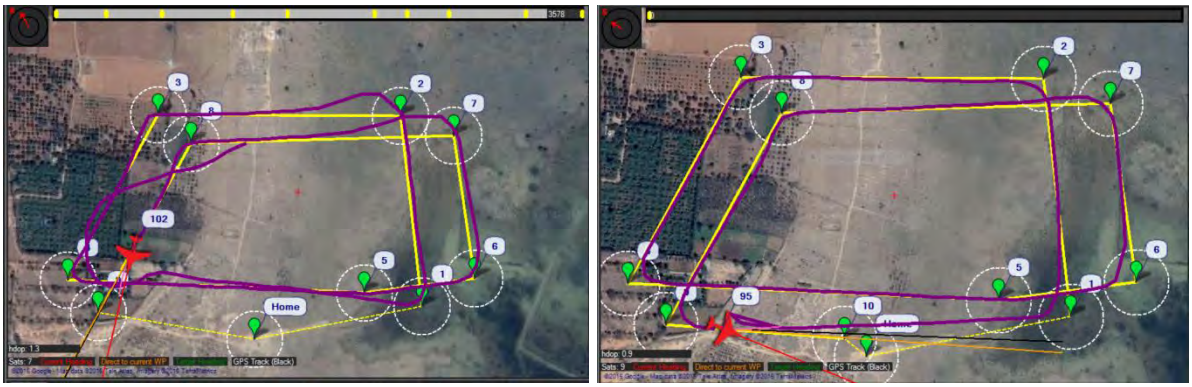

Fig.7. [*left***]** Waypoint tracking before tuning waypoint transition.
Fig.8. [*right*] Flight path tracking after tuning waypoint transition in winds gusting to 22 km/hr.

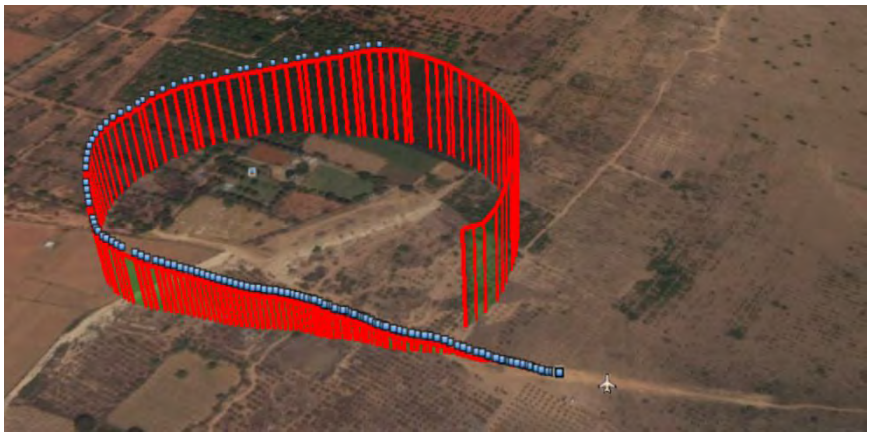

Fig.9. A plot of the UAS's position during an autonomous landing sequence showing an ideal glide slope and control over positioning.

3.2 Automatic Detection, Localization, and Classification

Image processing algorithms were initially developed using sample images obtained from static tests (80 m altitude, high noise environment), and then optimized using images from dynamic tests conducted during mission simulations.

3.2.1 Automatic Detection And Extraction Of Targets

The Saliency Detection algorithm was tested using a comprehensive variety of images that included different backgrounds (grass, mud, and tarmac) encountered during test flights. When passed through the aforementioned filters, the algorithm returned a large number of false positives by categorizing clumps of grass and random asymmetrical objects as potential targets. The thresholds in the filters were subsequently modified, and the rate of erroneous detection was reduced from 48% to 14%.

3.2 Colour Recognition

The primary factor found to interfere with successful colour recognition was the blurring of boundaries between the alphanumeric character and the background due to discretization during processing, which led to ambiguous outputs. An optimum threshold to categorize the entire visible spectrum into 16 distinct colours was determined by intensive testing using a variety of target images obtained in different lighting conditions.

3.2.3 Shape Classification

The shape classification algorithm was initially found to be unreliable due to its inability to reconstruct shapes from certain cropped targets (due to loss of clarity). This issue was resolved by adding provisions for linear extrapolation to completely reconstruct targets.

3.2.4 Localization

The results of the localization algorithm were verified using corresponding GPS coordinates obtained from Google APIs. The error rate of 12% was attributed to the performance of the geotagger module attached to the camera.

3.2.5 QR Code

The accuracy of the QR decoder depended on the clarity of the cropped target, and therefore, on the processing of the original image. It was tested using QR Codes of different resolutions, orientations and for varying distances. The success rate remained at a steady 24% during mission simulation flights.

Table 3: Test results of the ADLC algorithm for images captured at SUAS Competition 2015 and during mission simulations.

Original Image	Extracted Target	Localization	Classification	Remarks
		Latitude: 13.074830 Longitude: 77.766566 Orientation: 45.78	Shape: Triangle Colour: Blue Character: O Colour: Red	A localization error of 12% was obtained when compared with Google API values. The orientation was found to have an error of 7.45%.
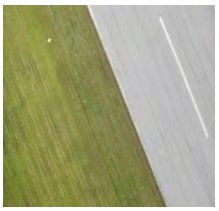		Latitude: 38.1470555268 Longitude: -76.4305308755 Orientation: 307.59	Shape: Cross Colour: White Character: E Colour: Blue	All target characteristics were determined correctly.
	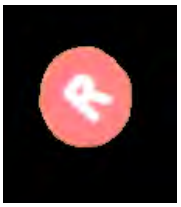	Longitude: -76.4305295628 Latitude: 38.1467153898 Orientation: 11.84	Shape: Circle Colour: Red Character: R Colour: White	All target characteristics were determined correctly.
	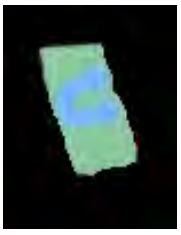	Latitude: 38.1457281621 Longitude: -76.4301433416 Orientation: 73.68	Shape: Trapezium Colour: Green Character: U Colour: Blue	Shape was incorrectly categorized as a Trapezium, instead of a Rectangle.

3.3 Sense, Detect and Avoid (SDA)

The obstacle avoidance algorithm was ground tested using hardware-in-the-loop simulations to pin-point required parametric changes to the algorithm, thus fine-tuning the algorithm to a flight-ready state. Intensive testing showed that the optimization algorithm used was capable of rerouting the UAS when presented with obstacle data and the original flight path.

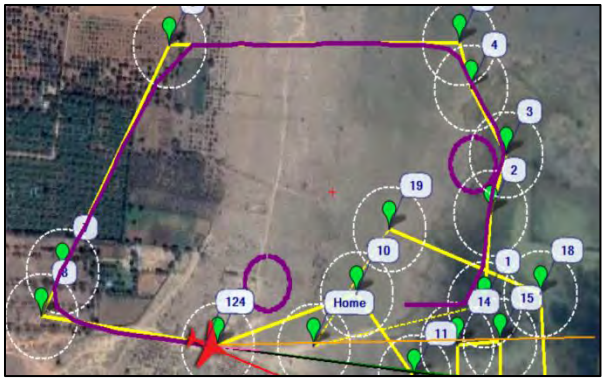

Fig.10. The modified flight path ensured obstacle avoidance with minimum deviation from the planned flight path. GPS positioning error was accounted for with obstacle admittance.

Fig.11.A. Obstacle (visualized using purple circles) penetration: Individual candidates moving too quickly.

Solution: An upper bound was set to the velocities of each candidate of the flock, and an appropriate time-step was chosen such that the maximum distance travelled between iterations did not exceed 50% of the diameter of the smallest obstacle.

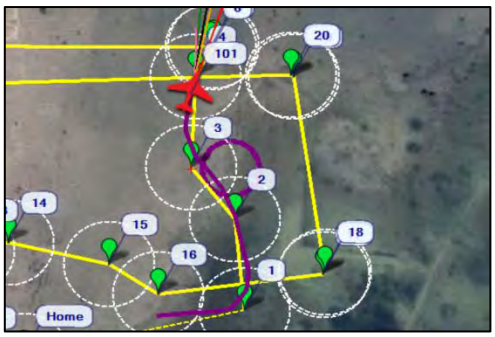

Fig.11.B. Unfavourable response of the UAS: Acute sharpness of generated paths and lack of consideration towards control system latency.

Solution: A simple low-pass filtering (an averaging filter with a window size of 5) was employed to smoothen the path.

3.4 SRIC

In order to establish and maintain connectivity with the SRIC server, the UAS was required to loiter at a radius which was within the beam width of the SRIC antenna. The loiter radius was calculated to be 69.28 m using the given beam angle of 60 degrees and the predetermined flight altitude of 120m. The UAS was tested at loiter radii as low as 50 m to ensure a stable link with the SRIC server. The upload and download tasks were successfully completed using SFTP.

3.5 Interoperability

The interoperability client has been tested across different networks with consistent data rates of 9-10 Hz. Initial problems involved the setup of the judge server, but with the help of developer support, a constant stream of telemetry data to the server at an average of 9 Hz was achieved. Further requirements such as display of server wall clock, submission of targets, and the acquisition of obstacle data, have been met using Python scripts for maximum compatibility. Data dropouts have occurred rarely, due to the use of networks with higher traffic, and this has been rectified.

3.6 Performance of Airframe and Power Systems

The airframe was loaded gradually to find the limits of the structure, and to identify flight characteristics at various loadouts. Initial testing revealed wing flexure exceeding acceptable limits with the wings visibly deforming under moderate G loading. The reinforced wings were tested with steep dives and banks exceeding dive and roll rates to be used by the FC to test the strength of the modified wings. The results showed that wing flexure was within acceptable limits, and was consistent with the flexure seen in wings with high aspect ratios.

The power draw was tested for multiple loadouts with 3 different propellers. Maximum performance was achieved with 10X6 propellers, with the propellers providing enough thrust for emergency manoeuvres. Initial tests showed power consumption exceeding expected values which was attributed to high throttle inputs and high speed flight at 20 m/s. The airframe was tested at a significantly lowered airspeed of 14 m/s which allowed for better imagery performance and longer flight times. Flight tests showed that the UAS was capable of 35 minutes of flight in full mission configuration, well above the maximum allowed 30 minute flight duration.

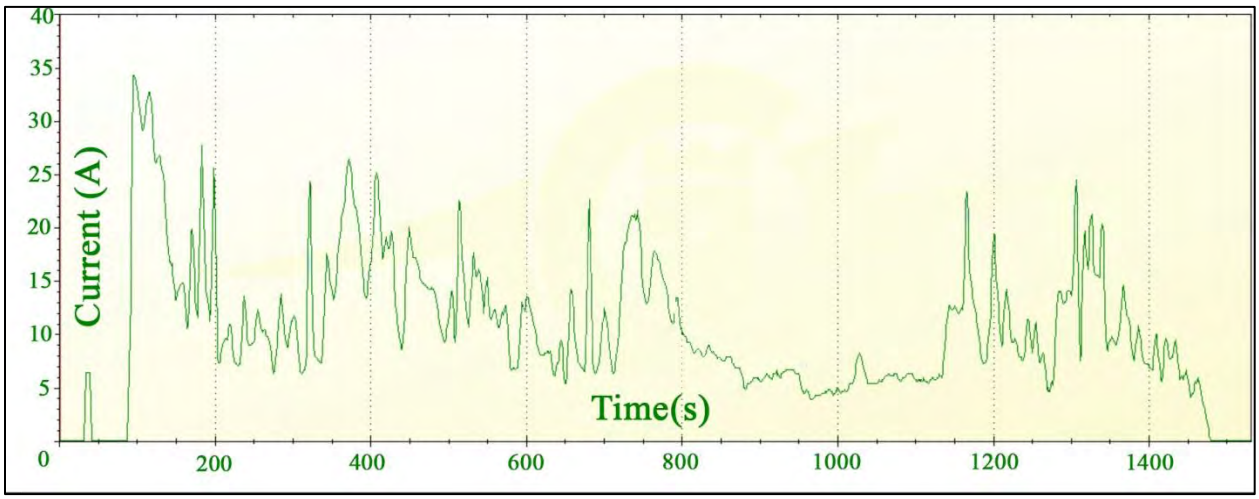

Fig.12. Current drawn v/s time: The graph shows an average current draw of 11 A per motor in autonomous flight, allowing for flight times of 35 minutes.

Tests in ambient temperatures of 100 F showed motor temperatures at 107 F, motor controller temperatures at 95.5 F, and battery temperature at 103 F after 25 minute flights. All operating temperatures were well within the limits specified by the manufacturers and confirmed that all systems were operating within their performance limits.

3.7 Flight Controller

FC performance was tested with flight plans consisting of steep banks with sharp changes in altitude, intended to test the limits of the airframe. Having determined the flight envelope, the PID control loop was tuned for the roll, pitch, and yaw. Testing was carried out to replicate full mission payload with winds gusting to 25 Km/h. Progressive tuning enabled waypoint capture and flight path tracking with the required accuracy. The Total Energy Control System (TECS) loop was tuned to power the airframe through high climb rates which ensured waypoint capture within altitude requirements. The airspeed sensor was calibrated and monitored regularly for erroneous readings that would affect autonomous flight, and specifically, autonomous landing.

3.8 Data Transfer

Data transfer rates were tested in high noise RF environments at ranges exceeding 550 m. Additionally, flight tests at maximum altitude were conducted to check datalink performance. Both tests showed an effective data transfer rate of 4 MB/s. The average time taken to transfer a 12 MP JPEG Fine image (6.8 MB) from the OBC to the GCS was found to be approximately 1.12 seconds.

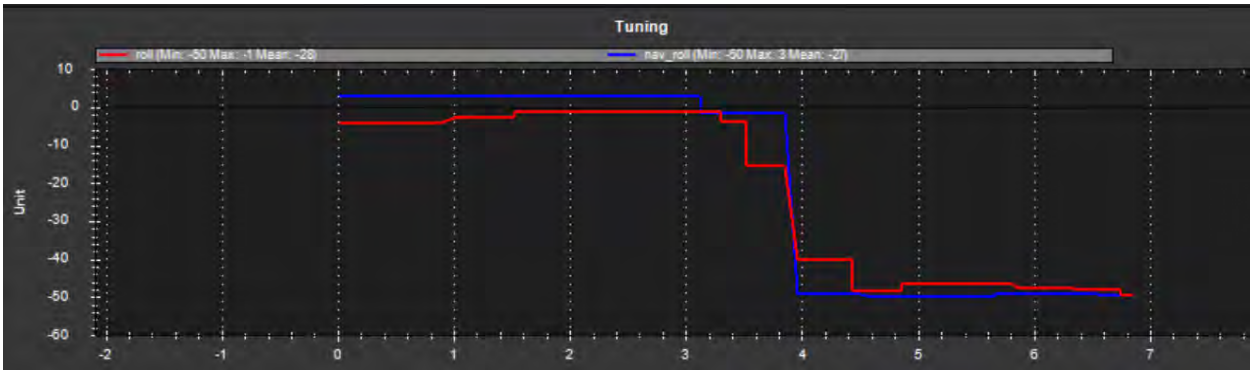

Fig.13. Actual Roll (red) and Commanded Roll (blue) v/s Time: The response curves for the roll axis showed the actual attitude following the demanded attitude closely. Response times were minimized to allow for optimum tracking without exceeding the structural limits of the airframe.

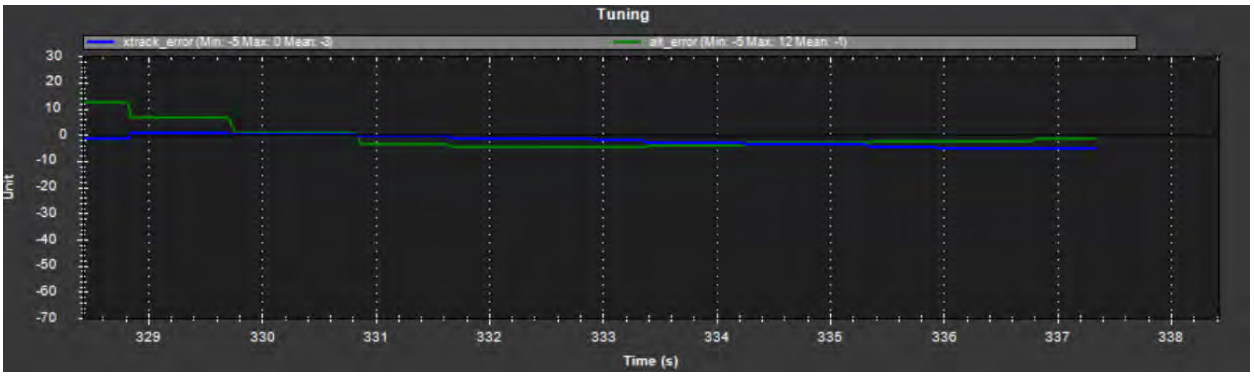

Fig.14. Acceptable crosstrack and altitude errors v/s time, in autonomous flight.

3.9 Performance of payload system

3.9.1 On Board Computer

The actual CPU usage for on-field operations during mission simulations never exceeded more than 48%. The maximum current drawn by the Odroid C1 was 598 mA, and the idle power consumption was between 1.7 W and 1.8 W. The performance of the Odroid C1 was initially tested using a benchmark suite, Sysbench, using certain configurations. The Sysbench configurations, however, were used to only test the maximum capabilities of the OBC.

> *Config: sysbench --num-threads=1 --test=cpu --cpu-max-prime=2000 run*
> *Total time: 23.8167s, total number of commands: 10000.*
> *Per-request statistics: min: 2.38ms, avg: 2.38ms max: 2.56ms.*
> *Threads fairness: events (avg/stddev): 10000.0000/0.00,*
> *Execution time (avg/stddev): 23.8075/0.00*

3.9.2 Imagery Performance

The camera was tested for both 12 MP and 24 MP options, with the 12 MP setting being chosen due to the lower transfer time per image. Multiple lenses were tested, with a 35 mm lens offering the best area coverage at minimum distortion. Different settings for ISO, aperture, and shutter speed were tested at different times of day in conditions varying from clear to cloudy skies to account for most possible weather conditions. The images obtained were of sufficient quality to allow manual operators and the ADLC algorithms to detect and classify targets.

3.10 Summary Of Test Results

Table 4. Summary of test results of mission simulations and likelihood of mission completion at SUAS 2016.

Mission Task	Mission Sub-Task	Success Rate		Expected Performance at SUAS 2016
		Threshold	Objective	
Autonomous Flight	Auto Flight	-	74%	Will meet all objectives
	Waypoint Navigation	-	100%	
	GCS Display	-	100%	
Search Area Task	Localisation	100%	58%	Will meet all objectives
	Classification (of QRC)	100%	78% (22%)	
	Imagery	-	100%	
	Autonomous Search	-	100%	
	Secret Message	-	n/a	
Automatic Detection, Localisation, and Classification	Localisation	-	44%	Will meet all objectives
	Classification (of QRC)	-	68% (22%)	
	False Alarm Rate (FAR)	-	24%	
Actionable Intelligence Task	Localisation and Classification	90%	58%	Will meet all objectives
Off-Axis Standard Target Task	n/a	-	n/a	Will not attempt
Emergent Target Task	In-flight Re-tasking	-	100%	Will meet all objectives
	Autonomous Search	-	100%	
	Target Identification	48%	34%	
Airdrop	n/a	-	n/a	Will not attempt
Simulated Remote Information Center (SRIC)	SRIC Upload & Download Task	-	78%	Will meet all objectives
	Autonomous SRIC Task	-	34%	
Interoperability	Download & Display Server Info, Time and Obstacles	94%	66%	Will meet all objectives
	Upload Target Details	-	64%	
Sense, Detect and Avoid (SDA)	Stationary Obstacle Avoidance	90%	82%	Will meet all objectives
	Moving Obstacle Avoidance	-	n/a	Will not attempt

4. Specific Safety Criteria for Systems and Operations

4.1 Safety Criteria for Systems

The major requirement for system design was the minimization of all possible points of failure. Every subsystem has been designed to avoid a cascaded failure in the event of subsystem failure.

The twin motor configuration allows for controlled flight in the unlikely event of partial propulsion failure. The probability of dual propulsion failure is highly unlikely owing to the low rates of failure on the motors and motor controllers. In the event of complete propulsion failure, the flight characteristics of the airframe allow for a controlled glide to a designated landing area.

The flight controller is equipped with a backup processor in the event of failure of the primary processor. Multiple failsafes set in the firmware allow for controlled flight and flight termination should the need arise. The flight controller is powered off a separate power line to ensure adequate supply of power during the entire mission. A Zener diode is used on the servo power rail to negate voltage spikes likely to be caused by the use of digital servos. A “glitch buster” capacitor is used to minimize power line noise and to provide reserve power to the servos and prevent “brown outs’ in the unlikely event that the 5A supply is inadequate. Capacitor banks are used to protect the speed controllers from being damaged by transitionary ripple currents. A detailed log of post flight temperatures and ripple currents has been maintained to gauge the health of the speed controllers. A maximum ripple voltage of 0.55 V, well below the safe limit of 1.48V as suggested by the manufacturer, was obtained.

The servos are powered by a dual redundant power supply. The use of two motor controllers has provided the UAS with two 5 A switching voltage regulators. The voltage regulators are run at voltages separated by 0.2 V through a barrier rectifier circuit to allow the regulator with the higher voltage to power the servos and FC. In the event of failure of one regulator, power will be supplied by the other regulator (dormant during normal conditions). The two voltages are within the acceptable ranges for all equipment to ensure optimum performance.

4.2 Safety Criteria for Operations

4.2.1 Field Checklists (Pre-flight and Post-flight)

Checklists are used by each sub team to ensure system readiness and safety before powering the UAS. Checklist items are checked by sub team leads and the safety officer to negate human error. Combined with the pre flight checks, the checklists have ensured optimum flight performance with no faults attributed to operator error. Detailed inspections of the UAS structure, wiring, and state are performed before and after every flight to check structural integrity, electrical connections, and system readiness. After a high stress event such as a crash landing, each sub team creates a report verifying the health of relevant systems and confirms peak performance.

4.2.2 Navigation system health Checks and Pre-arm checks

The use of a sensor fusion algorithm allows the FC to identify and correct erroneous sensor readings by determining a correction based on an experimentally determined ratio of the error in computed states to the error in measurements. Errors greater than thresholds set are communicated to the GCS operator, with backup sensor readings being used for navigation. Pre arm checks verify the operational reliability of the IMU, compass, gyroscopes, and the remote control system. A failure on any of the checks does not allow the propulsion and control systems to be armed. Minimum values for the Horizontal Dilution of Precision (HDoP) are set to allow autonomous flight only if the value is acceptable to negates positioning errors caused by incorrect GPS readings.

4.2.3 Designated tasks and chain of command

Each team member is assigned specific tasks on the field during setup and flight. Having been trained for their specific roles, team members were made capable of identifying problems. Repetitive practice drills drastically lowered human error and, as a result, made the whole system safer. These roles are assigned by the team captain for monitoring of on-field performance and to enable quick decision making. All decisions are passed up the chain, starting from field personnel, ending with the team lead.

4.3 Safety Risks and Mitigation Methods

Table 5. Summary of risk analysis and mitigation strategies.

Risk	Likelihood	Impact	Mitigation Strategy
Servo failure	Low	Loss of airframe in case of multiple failures.	Servo operation checked during checklist procedures. Use of servos with a factor of safety over 1.3 on load handling.
Loss of RC link	Low	Loss of control if in manual flight.	Use of a failsafe with a return to launch till control is regained. Receiver placement to minimize interference Provision of redundant power to the receiver.
Loss of one motor/ asymmetric propulsion failure	Low	Loss of thrust and unstable flight characteristics.	Pre-flight checklists to ensure no physical damage to motors. Post flight analysis to determine motor performance and identify potential signs of failure.
Loss of power to the flight controller	Low	Complete loss of control leading to a crash.	Supply of triple redundant power to the flight controller.
Incorrect wiring	Moderate	Non-functional systems.	Pre-flight checklist items to check for faulty wiring. Periodic maintenance to identify frayed wires, chafed insulation, or loose connectors.

5. Conclusion

Development for the SUAS 2016 presented a steep learning curve for Edhitha. A number of algorithms were explored during the development of the data processing and path finding algorithms, with the selected ones being optimized to the greatest possible extent. Staying true to the team's dedication to safety and reliability, subsystems have been rigorously tested and team members have been suitably trained ensure the success of the mission. With over 27 flight tests and two full mission simulations, Edhitha is confident in the UAS's ability to successfully meet the mission objectives at the SUAS 2016.

List of Team Members

Team Member	Role in Team
Ankan Dutta	Electrical & Software Subteam
Anmol Bhoj	Mechanical Subteam, Navigation Subteam
Arjun Jagdish Ram	Electrical & Software Subteam
Deborshi Goswami	Captain, Electrical and Software Subteam
Gandhar Kunte	Vice-Captain, Navigation Subteam
Gaurav Chhikara	Mechanical Subteam
Sushanth Jayanth	Mechanical Subteam
Sangharsh Bhustalimath	Safety Pilot, Mechanical Subteam
Vikram Kamath	Software Subteam

Faculty Advisor:	Prof. A. T. Venkatesh
Team Mentors:	Sharath Nairy Vishwanathan Ramanathan Vishnu B.N. Praneeta Mallela Sankha Karfa.